Journal of Dermatological Science 95 (2019) 119–122

Contents lists available at ScienceDirect

Journal of Dermatological Science

journal homepage: www.jdsjournal.com

Letter to the Editor

Alterations in connexin 26 protein structure from lethal keratitis-ichthyosis-deafness syndrome mutations A88V and G45E

To the Editor

Recent analysis of keratitis-ichthyosis-deafness (KID) syndrome patients correlated genotype (*GJB2* mutations p.A88V and p.G45E) with lethal clinical phenotype and identified that these patients have multiple organ system defects [1]. *GJB2* encodes connexin 26 (Cx26). Several biochemical experiments established that Cx26 has carbon dioxide (CO_2) sensing function, mediated by the carbamylation of Lys125 with subsequent salt bridge formation to Arg104 (from a neighboring Cx26 protomer) on the intracellular region of the Cx26 hemichannel [2,3]. Moreover, HeLa cells expressing $Cx26^{A88V}$ demonstrated hemichannels that lack sensitivity to CO_2 [3]. Since KID syndrome patients with lethal *GJB2* mutations have respiratory difficulties, we investigated using molecular modeling whether the CO_2-sensing mechanism of Cx26 might be altered by A88 V and G45E mutations. These mutations were modeled using the Cx26 crystal structure (PDB Code 2ZW3) [1,4]. The structural analyses described here help connect the biochemistry experiments with the clinical observations; they support an effect of the A88 V, but not the G45E, mutation on CO_2 sensing.

To understand how A88 V alters Cx26 structure and CO_2 sensing, we characterized the molecular interactions occurring around A88. A88 follows a proline (P87), which is highly conserved across connexins (Fig. 1a). P87 exists in the second transmembrane helix (TM2) of Cx26 where it induces a proline kink essential for the transduction of voltage gating [1,5]. This kink imposes unique steric constraints on TM2; it also exists in Cx32 [6]. Mutations to P87 in Cx26 [5] and to T86 or P87 in Cx32 [6] cause functional changes in voltage gating.

Given P87's proline kink and its imposed constraints, we determined whether $Cx26^{A88V}$ would physically clash with adjacent residues. We identified that substitution of any of the three possible valine rotamers at position 88 results in one or more steric clashes with neighboring residues (Fig. 1b,c). Specifically, V88 is detrimental to protein packing because it generates short interaction distances (ranging from 2.04 to 2.61 Å) between V88 Cγ atoms and either the S85 backbone carbonyl (rotamers 2 and 3) or the R143 guanidinium group NH2 (rotamers 1 and 2). This data suggests that the initial step towards altered Cx26 CO_2 sensing is V88 physically clashing with S85 and/or R143 because of the local structural environment created by P87 [7,8].

Analysis of the solvent accessible surface area (SASA) of Cx26 revealed that A88 is mostly buried within the protein core that is embedded in the lipid bilayer (17% SASA) (Fig. 1d,e). Furthermore, P87 and A88 on TM2, and R143 on TM3, exist in regions calculated to have high protein rigidity, meaning they help stabilize the Cx26 core (Fig. 1d). To avoid unfavorable stereochemistry in that core, $Cx26^{A88V}$ can only be accommodated if a compensatory rearrangement in the packing of transmembrane helices occurs during protein folding. Small changes in helical packing near V88 can lead simultaneously to repositioning of the helices distally. The distance between CO_2-sensing residues K125 and R104 ranges from 6.3 to 6.5 Å (from crystal structure) [1]. R104 exists on the distal intracellular aspect of TM2; TM2 also contains A88 proximally. Therefore, re-packing of the proximal region of TM2 to accommodate the sterically unfavorable A88 V may alter the distal TM2 positioning of R104 and disrupt the delicate stereochemistry with K125 that is needed for carbamate salt bridge formation and CO_2 sensing. This mechanism is supported by biochemical experiments demonstrating the precision of the K125-R104 interaction: 1) $Cx26^{K125R}$ mutation prevents carbamylation; 2) $Cx26^{R104A}$ mutation disrupts salt bridge formation; 3) neither $Cx26^{K125R}$ nor $Cx26^{R104A}$ display CO2 sensitivity [2]. Ala88 is conserved in CO_2-sensing connexins Cx26, Cx30, and Cx32, but not other connexins (Fig. 1a). This suggests alanine is stereochemically superior at position 88 for establishing proper structural chemistry at the CO_2-sensing residues.

In contrast, lethal KID syndrome mutation G45E is unlikely to alter CO_2 sensing. G45 exists at the junction of TM1 and the first extra-cellular loop (E1) (Fig. 2a), not in the rigid Cx26 core (Fig. 1d). This region helps regulate voltage sensing [4,9]. Whereas A88 V is predicted to alter protein conformation, G45E changes the charge distribution and pore diameter of the connexin channel (Fig. 2a–c). Since G45 is at the solvent-exposed surface of the channel pore, mutation to glutamate reduces the pore diameter around the connexin hemi-channel. Based on electrostatic potential calculations, G45E also adds negative charge potential to the pore lining, possibly affecting electrostatic interactions within the channel (Fig. 2c). From a structural perspective, CO_2 sensing at the channel's intracellular surface should not be affected by this solvent-exposed pore-lining mutation. Structural analysis suggests G45E alters a different critical aspect of Cx26 function (charge selectivity and pore diameter), which could be clinically detrimental independent from CO_2 sensing.

To investigate changes in Cx26 stability caused by A88 V and G45E, we utilized PoPMuSiC [10] to predict change in folding free energy (ΔΔG, kcal/mol) of Cx26 based on the wild-type structure and single-site mutations. Of seven Cx26 mutations analyzed, six are predicted to have destabilizing structural effects (positive ΔΔG: S17 F, M34 T, A40 V, D50 N, V84 L, A88 V) and one a stabilizing structural effect (negative ΔΔG: G45E) (Fig. 2d). PoPMuSiC is predicated on the fact that mutations to residues buried within the protein interior will have greater consequence to protein stability than mutations to highly solvent-accessible

https://doi.org/10.1016/j.jdermsci.2019.07.002

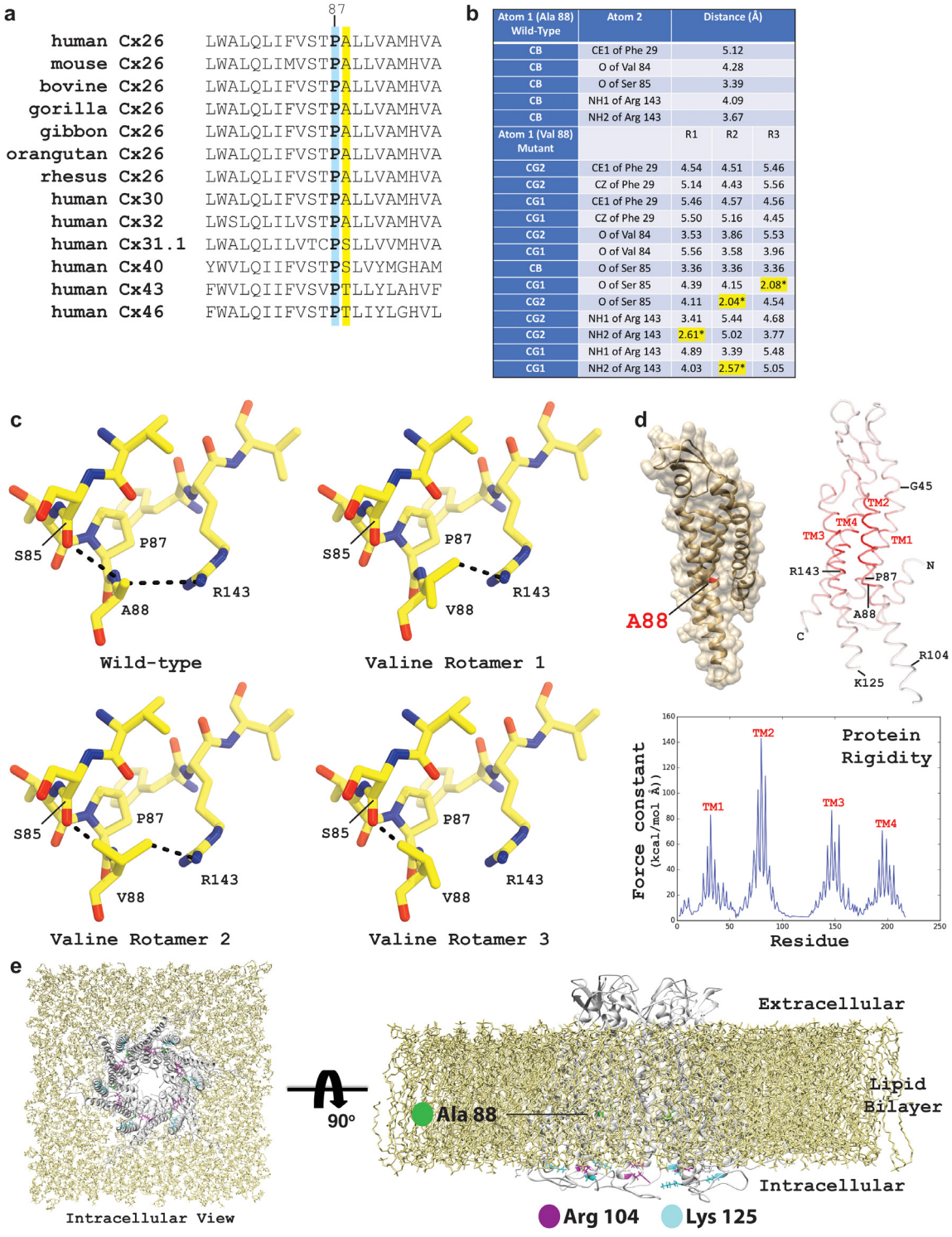

Fig. 1. Lethal connexin 26 A88 V mutation disrupts transmembrane helix 2 hydrophobic packing. (a) Multiple sequence alignment of connexins demonstrating complete conservation of P87 (blue). The CO_2-sensing connexins (26, 30, 32 [7]) conserve A88, whereas other connexins do not (yellow). (b) Atomic distances between position 88 and the closest atoms of surrounding residues in Cx26. CB, beta carbon; CE, epsilon carbon; CG, gamma carbon; O, carbonyl oxygen; NH, amino group; R1-R3, valine rotamers 1-3. Distances are based on subunit A of the Cx26 hexamer (PDB Code 2ZW3) without modeling of hydrogen atoms. An asterix (*) denotes major structural clashes, which were validated using Molprobity analysis of the mutated structure with hydrogen atoms. (c) Chemical structure of the residues surrounding P87 and A88 in wild-type Cx26 compared to the three possible valine rotamers in a $Cx26^{A88V}$ mutant. All positions of valine have steric clashes that would force protein re-packing. (d) The Cx26 wild-type protomer is depicted as a ribbon diagram and partially transparent molecular surface, with A88 highlighted in red, demonstrating A88 is buried within the protein (upper left). Protein rigidity, expressed as a force constant, was calculated across all Cx26 residues using ProPHet and four regions of higher rigidity were identified within the transmembrane (TM) helices (TM1: L25-W44; TM2: H73-A88; TM3: S139-Y158; TM4: K188-N206) (bottom). Protein rigidity was plotted onto a ribbon diagram of Cx26 (upper right) and colored (white, low rigidity; red, high rigidity) to visualize that P87, A88, and R143 lie within the highly rigid Cx26 core whereas G45 does not. (e) The Cx26 hemichannel embedded in a lipid bilayer viewed from an intracellular (left) and perpendicular (right) perspective. A88 exists on a helix within the lipid bilayer, while the R104 and K125 residues involved in CO_2 sensing reside intracellularly. How exactly A88 V affects the distal position of TM2 (including R104) is challenging to model *in silico*. Energy minimization algorithms excel at removing steric clashes around local energy minima, but cannot accurately predict larger protein conformation changes induced by amino acid mutation. Due to these limitations, crystal structures of Cx26 mutants are needed to understand the structural changes at CO_2-sensing sites.

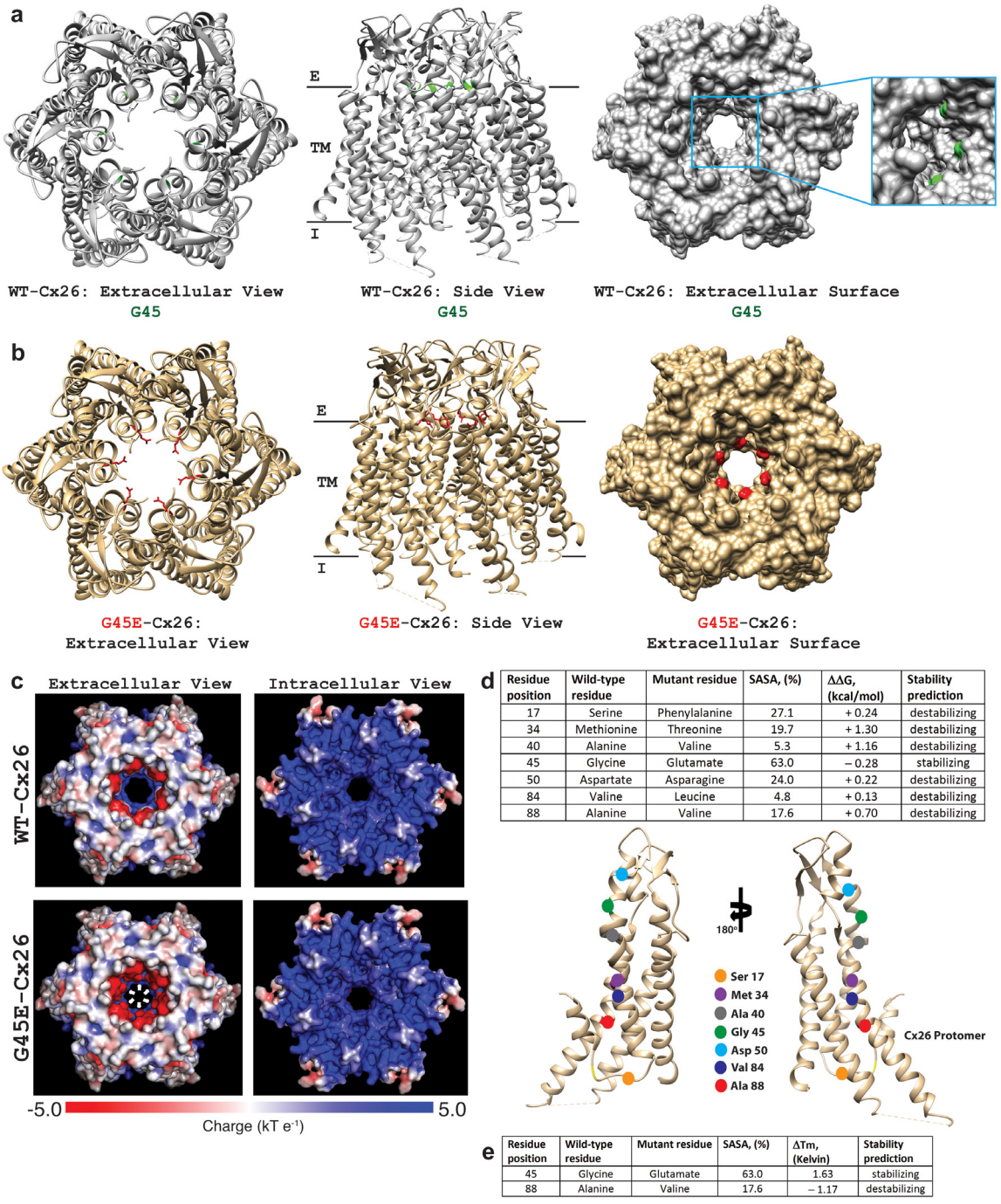

Residue position	Wild-type residue	Mutant residue	SASA, (%)	ΔΔG, (kcal/mol)	Stability prediction
17	Serine	Phenylalanine	27.1	+ 0.24	destabilizing
34	Methionine	Threonine	19.7	+ 1.30	destabilizing
40	Alanine	Valine	5.3	+ 1.16	destabilizing
45	Glycine	Glutamate	63.0	− 0.28	stabilizing
50	Aspartate	Asparagine	24.0	+ 0.22	destabilizing
84	Valine	Leucine	4.8	+ 0.13	destabilizing
88	Alanine	Valine	17.6	+ 0.70	destabilizing

e

Residue position	Wild-type residue	Mutant residue	SASA, (%)	ΔTm, (Kelvin)	Stability prediction
45	Glycine	Glutamate	63.0	1.63	stabilizing
88	Alanine	Valine	17.6	− 1.17	destabilizing

Fig. 2. Lethal connexin 26 G45E mutation alters channel pore diameter and charge. (a) The wild-type Cx26 crystal structure is presented as ribbon diagrams as follows: orientations viewing the channel from the extracellular compartment (left) or side-view (center); it is also presented as a molecular surface viewing the channel from the extracellular compartment (right). A zoomed and rotated (by 20° about the y-axis) view of the channel pore is shown (right) in order to visualize the small and non-protruding glycine residues (green). G45 from all 6 monomers of the hexameric hemichannel are colored green; they are difficult to visualize at the E/TM junction because glycine lacks a side chain moiety. (b) $Cx26^{G45E}$ structure presented in the same orientations as for **panel a**. Because the glutamate residue (red) is larger than the glycine, there is decrease in the channel diameter at the E/TM junction. (c) Electrostatic potential mapped onto the molecular surface of the Cx26 wild-type structure (top) and $Cx26^{G45E}$ structure (bottom) demonstrating increased negative electrostatic potential (red) lining the extracellular portion of the channel (left images), but no difference in the intracellular aspect of the channel which has positive electrostatic potential (blue). White arrows indicate G45E residues (bottom left). E, extracellular region; TM, transmembrane region; I, intracellular region. Electrostatics were calculated using PDB2PQR and Adaptive Poisson-Boltzmann Software (APBS). (d) PoPMuSiC analysis of how seven patient-derived single-site mutations of Cx26 alter protein folding free energy (ΔΔG) and stability (top). The locations of the mutations are mapped onto a Cx26 protomer (bottom). The mutation predicted to stabilize the Cx26 structure (G45E) occurs in a residue with a high solvent accessible surface area. Mutations predicted to destabilize the Cx26 structure occur in residues with low solvent accessible surface area, and therefore are more likely to disrupt internal protein packing. Protein structure alterations will not necessarily impact CO_2 sensing, depending on location and degree of structure perturbation. (e) HoTMuSic analysis of how A88 V and G45E mutations change the melting temperature (ΔTm) of Cx26. A88 V is destabilizing to Cx26 because it lowers the melting temperature (negative ΔTm), whereas G45E is stabilizing to Cx26 because it raises the melting temperature (positive ΔTm).

residues. G45 has the highest solvent accessibility of the residues analyzed (63%), suggesting mutations at Cx26 position 45 are less likely to disturb overall protein structure. To corroborate these findings, we also analyzed the change in protein melting temperature (ΔTm, Kelvin) due to A88 V or G45E mutation using HoTMuSiC (Fig. 2e). Calculations show G45E raising Tm (increased Cx26 stability), whereas A88 V lowers Tm (decreased Cx26 stability).

In conclusion, ΔΔG and ΔTm analyses concur with our structural analysis that A88 V is a destabilizing mutation to Cx26. However, data that G45E is stabilizing suggests that A88 V and G45E cause lethal pathophysiology from distinct biochemical mechanisms. This is consistent with our clinical observations that patients with lethal KID syndrome mutations demonstrate abnormalities in many organ systems [1], and suggests that respiratory difficulties can occur from other mechanisms besides CO_2 sensing.

Funding sources

NIH/NIAMS, Dermatology Foundation.

Acknowledgements

This work was supported by a Dermatology Foundation Career Development Award (to C.G.B.), an NIH/NIAMS Dermatology Training Grant to Yale T32 AR007016 (to C.G.B., E.L.; PI: Richard Edelson), and an NIH/NIAMS grant K08-AR070290 (to C.G.B.).

References

[1] E. Lilly, C.G. Bunick, A.M. Maley, S. Zhang, M.K. Spraker, A.J. Theos, K.L. Vivar, L. Seminario-Vidal, A.E. Bennett, R. Sidbury, Y. Ogawa, M. Akiyama, B. Binder, S. Hadj-Rabia, R.A. Morotti, E.J. Glusac, K.A. Choate, G. Richard, L.M. Milstone, More than keratitis, ichthyosis, and deafness: multisystem effects of lethal GJB2 mutations, J. Am. Acad. Dermatol. 80 (3) (2019) 617–625.

[2] L. Meigh, S.A. Greenhalgh, T.L. Rodgers, M.J. Cann, D.I. Roper, N. Dale, CO_2directly modulates connexin 26 by formation of carbamate bridges between subunits, Elife 2 (2013)e01213.

[3] L. Meigh, N. Hussain, D.K. Mulkey, N. Dale, Connexin26 hemichannels with a mutation that causes KID syndrome in humans lack sensitivity to CO_2, Elife 3 (2014)e04249.

[4] S. Maeda, S. Nakagawa, M. Suga, E. Yamashita, A. Oshima, Y. Fujiyoshi, T. Tsukihara, Structure of the connexin 26 gap junction channel at 3.5 A resolution, Nature 458 (7238) (2009) 597–602.

[5] T.M. Suchyna, L.X. Xu, F. Gao, C.R. Fourtner, B.J. Nicholson, Identification of a proline residue as a transduction element involved in voltage gating of gap junctions, Nature 365 (6449) (1993) 847–849.

[6] Y. Ri, J.A. Ballesteros, C.K. Abrams, S. Oh, V.K. Verselis, H. Weinstein, T.A. Bargiello, The role of a conserved proline residue in mediating conformational changes associated with voltage gating of Cx32 gap junctions, Biophys. J. 76 (6) (1999) 2887–2898.

[7] R.T. Huckstepp, R. Eason, A. Sachdev, N. Dale, CO_2-dependent opening of connexin 26 and related β connexins, J. Physiol. 588 (Pt. 20) (2010) 3921–3931.

[8] R.T. Huckstepp, R. id Bihi, R. Eason, K.M. Spyer, N. Dicke, K. Willecke, N. Marina, A.V. Gourine, N. Dale, Connexin hemichannel-mediated CO_2-dependent release of ATP in the medulla oblongata contributes to central respiratory chemosensitivity, J. Physiol. 588 (Pt. 20) (2010) 3901–3920.

[9] T. Kwon, B. Roux, S. Jo, J.B. Klauda, A.L. Harris, T.A. Bargiello, Molecular dynamics simulations of the Cx26 hemichannel: insights into voltage-dependent loop-gating, Biophys. J. 102 (6) (2012) 1341–1351.

[10] Y. Dehouck, A. Grosfils, B. Folch, D. Gilis, P. Bogaerts, M. Rooman, Fast and accurate predictions of protein stability changes upon mutations using statistical potentials and neural networks: PoPMuSiC-2.0, Bioinformatics 25 (19) (2009) 2537–2543.

Evelyn Lilly[a,1], Michael Strickler[b,c,1], Leonard M. Milstone[d], Christopher G. Bunick[c,d,*]
[a]Department of Dermatology, Massachusetts General Hospital, Harvard Medical School, Boston, MA, USA, [b]Yale Center for Research Computing, Yale University, New Haven, CT, 06520, USA, [c]Department of Molecular Biophysics and Biochemistry, Yale University, New Haven, CT, 06520, USA, [d]Department of Dermatology, Yale University, New Haven, CT, 06520, USA
[1]These authors contributed equally to this work.

* Corresponding author at: 333 Cedar St., LCI 501, PO Box 208059, New Haven, CT 06520-8059, USA.
E-mail address: christopher.bunick@yale.edu (C. Bunick).

Received 18 March 2019
Received in revised form 23 June 2019
Accepted 4 July 2019